CXC Chemokine Receptor-4 Antagonist Blocks Both Growth of Primary Tumor and Metastasis of Head and Neck Cancer in Xenograft Mouse Models

Younghyoun Yoon,[1] Zhongxing Liang,[1] Xin Zhang,[1] Mison Choe,[1] Aizhi Zhu,[1] Heidi T. Cho,[1] Dong M. Shin,[1] Mark M. Goodman,[2] Zhuo (Georgia) Chen,[1] and Hyunsuk Shim[1,2]

[1]Department of Hematology/Oncology, Winship Cancer Institute and [2]Department of Radiology, Emory University, School of Medicine, Atlanta, Georgia

Abstract

Squamous cell carcinoma of the head and neck (SCCHN) metastasizes to the lymph nodes and lungs. We have generated previously an orthotopic mouse model for head and neck metastasis and did *in vivo* selection of SCCHN cells through four rounds of serial metastases. A subpopulation of 686LN cells with high metastatic potential (686LN-Ms) was isolated. When the highly metastatic cells were compared with their low metastatic parental cells (686LN-Ps), we found that CXC chemokine receptor-4 (CXCR4) mRNA levels were significantly higher in the 686LN-Ms cells than the 686LN-Ps cells. Interestingly, the metastatic subclones had lost epithelial morphology and acquired mesenchymal features, which were maintained during cell expansion *in vitro*. This was featured by decreased E-cadherin and involucrin and increased vimentin and integrin β_1. These results imply that CXCR4 and epithelial-mesenchymal transition markers can be potential biomarkers to identify the subpopulation of cells with high metastatic potential. Using the orthotopic SCCHN animal model, we showed that anti-CXCR4 treatment suppressed primary tumor growth by inhibiting tumor angiogenesis and prevented lung metastasis. Because the reduction of metastasis seen in the treated group could have resulted from 2-fold reduction in primary tumor size compared with that in the control group, we examined the effects of the CXCR4 antagonist in an experimental metastatic animal model in which 686LN-Ms cells were i.v. injected. 686LN-Ms cells failed to metastasize in the CXCR4 antagonist-treated group, whereas they metastasized to the lungs in the control group. Our data indicate that CXCR4 is an important target to inhibit tumor progression in SCCHN. [Cancer Res 2007;67(15):7518–24]

Introduction

Squamous cell carcinoma (SCC), a malignant tumor of epithelial origin, represents >90% of all head and neck cancers.[3] In the United States, SCC of the head and neck (SCCHN) comprises ∼4% of all malignancies and is seen more frequently in men than in women. Tobacco and alcohol are major contributors to the development of this type of cancer. Although lymph node metastases are much more common in SCCHN patients (∼60%), up to 20% to 25% of patients with SCCHN develop distant metastatic disease where the main sites of metastases are the lungs, liver, and bone (1). SCCHN patients without nodal and distant metastases have a more favorable prognosis than their counterparts.[3]

Chemokines are secreted proteins that act in a coordinated fashion with cell surface proteins, including integrins, to direct the homing of various subsets of hematopoietic cells to specific anatomic sites (2–5). One such chemokine receptor, CXC chemokine receptor-4 (CXCR4), is also a major coreceptor for the entry of CXCR4-tropic human immunodeficiency virus, which causes rapid depletion of naive CD4$^+$ T cells during late stages of infection (6–9). Stromal cell-derived factor-1 (SDF-1) is a chemokine that interacts specifically with CXCR4. When SDF-1 binds to CXCR4, the complex activates pertussis toxin-sensitive Gα_I protein–mediated signaling (10). The interaction between SDF-1 and CXCR4 has been shown to direct cells to organ sites with high levels of SDF-1 expression, suggesting that this interaction plays a key role in the chemotaxis and homing of metastatic cells. Furthermore, SDF-1 is highly expressed in the lymph nodes and lungs, which are common destinations for SCCHN metastasis. Therefore, interruption of the interaction between CXCR4 and SDF-1 may provide a means of inhibiting the metastatic process.

The CXCR4/SDF-1 interaction has been shown to play a role in tumor angiogenesis (11). SDF-1 has been reported to influence the secretion of vascular endothelial growth factor (VEGF) and vice versa (12–15). Neutralizing antibodies to SDF-1 inhibited basic fibroblast growth factor– and VEGF-dependent neovascularization *in vivo*. Thus, these results indicate that the CXCR4/SDF-1 interaction may be critically involved in the regulation of angiogenesis.

Previously, we reported on the use of a peptide-based CXCR4 antagonist TN14003 as an imaging probe as well as an inhibitor of CXCR4/SDF-1–mediated metastasis in breast cancer. We also showed that this antagonist blocked the CXCR4 receptor by competing with its ligand SDF-1 (16).

We established metastatic SCCHN cell lines from a poorly metastatic parental cell line by three rounds of *in vivo* selection using a lymph node metastatic xenograft mouse model (17). Recently, we have further developed the highly metastatic SCCHN subclones by one additional round of *in vivo* section using the same model. We found that CXCR4 was elevated in all metastatic SCCHN clones when compared with their parental cells. Therefore, we investigated the effect of blocking CXCR4 function on SCCHN

[3] www.emedicine.com/plastic/topic376.htm

progression in both orthotopic and experimental animal models to examine the role of CXCR4 in both primary tumor growth and lung metastasis.

Materials and Methods

Cell culture. The human SCC cell line 686LN and its derivatives, nonmetastatic clones 686LN-Ps and metastatic clones 686LN-Ms, were cultured in 5% CO_2 at 37°C in DMEM/F-12 (Invitrogen) supplemented with 10% fetal bovine serum (Sigma), 50 units/mL penicillin, and 50 μg/mL streptomycin (Invitrogen).

Northern and Western blot analyses. For Northern blot analysis, total RNA (15 μg) was prepared with Trizol (Invitrogen) according to the manufacturer's instruction and loaded on a 1.4% agarose-formaldehyde gel. After transferring to nitrocellulose, the blot was probed with ^{32}P-labeled CXCR4 fragments (Genbank accession no. AI920946) and later washed once in 2× SSC (1× SSC is 0.15 mol/L NaCl plus 0.015 mol/L sodium citrate)-0.5% SDS for 30 min at room temperature and thrice in 0.2× SSC-0.5% SDS for 30 min at 50°C. For Western blot analysis, equivalent concentrations of total cellular proteins were resolved by SDS-PAGE (10% gel) and subjected to immunoblot analysis using polyclonal rabbit anti-CXCR4 antibody (Ab-2; EMD Biosciences) and a monoclonal mouse anti-β-actin (Sigma).

F-actin immunostaining. For immunofluorescence detection of F-actin, cells on a slide chamber were fixed for 15 min in 3.8% paraformaldehyde, washed in PBS, and permeabilized in 0.1% Triton X-100 for 3 min. Then, cells were incubated in Alexa Fluor 488 phalloidin in 1% bovine serum albumin in PBS (1:40; Invitrogen) for 20 min at room temperature, washed in PBS, incubated with propidium iodide (1:2,000) for 3 min, washed again, and mounted in an antifade mounting solution (Invitrogen); the samples were analyzed on a Nikon Eclipse E800 microscope.

Reverse transcription-PCR. Preparation of total RNA and reverse transcription-PCR (RT-PCR) was carried out as described previously (16). The human Snail-specific primers for 207 bp are 5′-TTTACCTTCCAG-CAGCCCTA and 3′-CCACTGTCCTCATCTGACA (Genbank accession no. AF131208), the primers for Twist are 5′-ATTAATAATAACGTCACACTTG and 3′-CGAAATTAATACGACTCACTAT (Genbank accession no. NM000474), and the primers for Slug are 5′-TGCAATAAGACCTATTCTACGTTCTC and 3′-CCCAGGCTCACATATTCCTT (Genbank accession no. U97060). For RT-PCR of mouse lungs, the total RNA was prepared from three slices (20 μm each slice) of frozen mouse lungs with Trizol (Invitrogen) according to the manufacturer's instruction. The human CXCR4-specific primers for 149 bp are 5′-GAACCCTGTTTCCGTGAAGA and 3′-CTTGTCCGTCATGCTTCTCA (Genbank accession no. NM003467), and the primers for β-actin are 5′-GACAGGATGCAGAAGGAGAT and 3′-TGCTTGCTGATCCACATCTG (Genbank accession no. X00351).

DNA microarray analysis. DNA microarray analysis was done as described in our previous publication (17). In brief, total RNA was prepared with Trizol. DNA microarray hybridization and scanning were done by the University of Pittsburgh Cancer Institute DNA Array Lab using the Affymetrix GeneChip HG-U133A. gcRMA in Bioconductor[4] was used for probe analysis and normalization of the microarray data. Statistical analysis (one-way ANOVA), false discovery rate calculation ($q < 0.001$), and fold changes filter (>1.5) were sequentially done to select the most significantly altered genes.

Antagonist and control peptide synthesis. The CXCR4 antagonist TN14003 and its control peptide were synthesized as described previously (16). The control peptide does not bind to CXCR4 protein.

Animal experiments. Orthotopic animal experiments were done on 6- to 8-week-old nude female mice (Taconic Farms) with six animals per group. We stably transfected the metastatic 686LN cells with the luciferase gene (pGL$_2$-control from Promega) for *in vivo* tracking purposes. The orthotopic metastatic SCCHN mouse model was described in our previous

publication (18). In brief, nude mice were injected submandibularly with 5×10^5 SCCHN cells suspended in 50 μL PBS to mylohyoid muscle and tumor growth was followed by noninvasive bioluminescence imaging (BLI). On the 8th day following the tumor cell injection, we took BLI images of mice and divided them equally into two groups with the same average tumor size in each group, one for TN14003 treatment and another for control peptide injection. I.p. treatment with TN14003 and the control peptide (2 mg/kg) started on the 8th day after the tumor injection and lasted for 27 days. At the termination of experiments (35 days following the tumor cell injection), tumor tissues, lungs, and other organs were collected.

For the experimental metastatic animal model, metastatic 686LN tumor cells (2×10^6) suspended in a volume of 100 μL HBSS were injected through the tail vein of nude mice. Cells were mixed *in vitro* before injection in 100 nmol/L TN14003 for a few minutes. During a 30-day treatment period, animals were i.p. injected with either TN14003 or its control peptide (2 mg/kg) thrice weekly beginning from day 2. The animals were sacrificed 30 days after the tumor cell injection. Mice were imaged on the micro–positron emission tomography (microPET) scanner with [^{18}F]fluorodeoxyglucose (FDG), before the sacrifice. Whole lung tissues were harvested in OCT (Fisher Scientific) compound and snap frozen in liquid nitrogen. The frozen lung tissues were sectioned to generate total RNA that was subjected to RT-PCR with human CXCR4 primers to confirm the imaging data. All protocols for animal studies were reviewed and approved by the Institutional Animal Care and Use Committee at Emory University.

MicroPET imaging of lung metastasis. MicroPET studies were done using six mice from two groups: control and CXCR4 antagonist treated. One hour after tail vein injections of 150 μCi [^{18}F]FDG in a volume of 150 μL, the animals were anesthetized and placed on a platform inside the microPET scanner. Mouse microPET images were acquired on the Concord P4 microPET scanner that has 26 cm transaxial and 8 cm axial fields of view. Fifteen-minute images were acquired using microPET with the long axis of the mouse parallel to the long axis of the scanner. Quality control scans were done before scanning any animals and the scanner was calibrated by analyzing a uniform phantom with similar activity concentrations as in the animals. Images were reconstructed with measured attenuation correction (20-min scan with a Ge-68 point source that spirals through the field of view). The attenuation data were then reconstructed into an image that was further segmented into tissue, air, and bone regions to which known attenuation coefficients were assigned. The resulting images were quantitatively calibrated and had a 2 mm isotropic resolution. Data acquisition and processing, including image reconstruction, image display, and analyses were done with the ASIPro program provided by Concorde Microsystems. A pixel region of interest was outlined in the regions of increased FDG uptake, and after correcting for radioactive decay, the maximal standardized uptake value (SUV_{max}) was semiquantitatively calculated according to Truong et al. (19). [^{18}F]FDG was synthesized by the method described by Hamacher et al. (20) at specific activities of ∼ 5,000 Ci/mmol.

Histologic evaluation. For the orthotopic animal model, mouse lungs were collected and fixed in 10% buffered formalin at the termination of the experiment. The formalin-fixed lungs were paraffin embedded and the entire lung was sectioned into 6-μm slices and every 10th section was stained with H&E to evaluate the presence or absence of lung metastasis. Incidences of metastases in each mouse were evaluated by two researchers independently (Y.Y. and M.C.). The primary tumors were fixed in buffered formalin and paraffin embedded. The tumors were sectioned into 6 μm and the tumor tissue sections were heated at 58°C for 30 min. These specimens were washed with xylene thrice for 5 min each followed by washes with 100%, 95%, and 75% ethanol and rinsed with PBS. To block nonspecific binding, the samples were incubated in avidin-block and biotin-block sequentially. The antimouse CD31 antibody (0.6 μg/mL; BD Biosciences) was applied to tissue sections and the samples were further incubated for 45 min in a humidified chamber at room temperature. The slides were washed thrice with PBS and incubated in a secondary antibody (1:150 dilution; Jackson ImmunoResearch Laboratories) for 30 min at room temperature. The samples were analyzed on a Nikon Eclipse E800 microscope.

For the experimental model for lung metastasis, animal lungs were snap frozen in OCT compound in liquid nitrogen, sectioned, and fixed in ice-cold acetone and maintained at −80°C. RT-PCR of CXCR4 was carried out as described previously (16).

Statistical analysis. All statistical significances were determined by Student's *t* test.

Results

CXCR4 levels are elevated in metastatic SCCHN subclones. We reported previously the generation of subclones of the SCCHN cell line 686LN by *in vivo* selection through three rounds of serial metastases in the SCCHN orthotopic animal model (17). Recently, a subpopulation of 686LN cells with high metastatic potential (686LN-Ms) was generated by one additional round of *in vivo* selection. These were compared with their low metastatic parental cells (686LN-Ps) to determine whether CXCR4 expression levels correlate with the metastatic potential of these subclones. It was found that the metastatic clones express significantly higher CXCR4 levels than the parental clones (686LN-Ps), in which CXCR4 mRNA levels were not detectable as determined by Northern blot analysis (Fig. 1*A*). Furthermore, a higher protein expression of CXCR4 in metastatic clones compared with their parental clones was determined by Western blot analysis (data provided in supplemental section).

Metastatic SCCHN cells have poorly differentiated morphology. The metastatic clones were found to have significantly different morphology compared with the nonmetastatic clones. Phalloidin staining showed a striking difference in the actin cytoskeleton and in cell adhesion (Fig. 1*B*). The metastatic cells failed to organize actin stress fibers and only loosely adhered to the substratum, whereas the parental cells adhered normally to the substratum, indicating that the metastatic clones had lost key characteristics of epithelial cells. In addition, we sought to determine the protein expression levels of epithelial-mesenchymal

transition (EMT) biomarkers. The parental cells expressed high levels of involucrin and E-cadherin, but low levels of vimentin and integrin β_1, whereas the metastatic clones showed the opposite pattern (Fig. 1*C*). We then determined the levels of EMT-inducing transcription factors, such as Slug, Snail, and Twist. These are critical regulators of the expression of tumor suppressors, such as E-cadherin. We found that Snail was significantly up-regulated in four of five metastatic clones compared with their nonmetastatic counterparts, as shown by RT-PCR (Fig. 1*D*), whereas Slug and Twist were not up-regulated in metastatic clones (data not shown).

Differential expression pattern of chemokine and interleukin family genes. To determine differences between metastatic and nonmetastatic cells in expression levels of chemokines, interleukins (IL), and their receptors, we did DNA microarray analysis using the Affymetrix GeneChip (17). Based on their significant difference in CXCR4 levels, we predicted that other chemotactic signaling proteins would be differentially expressed between the metastatic and nonmetastatic cells. Total RNAs from these cells were hybridized to the Affymetrix GeneChip (HG-U133A) containing gene fragments of common chemokines, ILs, and their receptors. After normalization, the data were filtered by one-way ANOVA analysis and cutoff by false discovery value ($q < 0.001$). The differentially expressed chemokines, ILs, and their receptors are listed in Table 1. *CXCR4* and *IL-6* were significantly elevated in the metastatic cells compared with their counterpart. Both genes have been implicated in metastatic progression of cancers.

Blocking CXCR4 suppresses primary tumor growth of SCCHN. As an *in vitro* model system for metastasis, we used a Matrigel invasion chamber (Becton Dickinson). SDF-1α was added to the lower chamber to induce SCCHN cells to invade through the Matrigel. With 200 ng/mL SDF-1α in the bottom chamber, significantly greater numbers of metastatic SCCHN cells responded to the chemoattractant and migrated into the bottom chamber than in the absence of SDF-1. This SDF-1–mediated invasion was
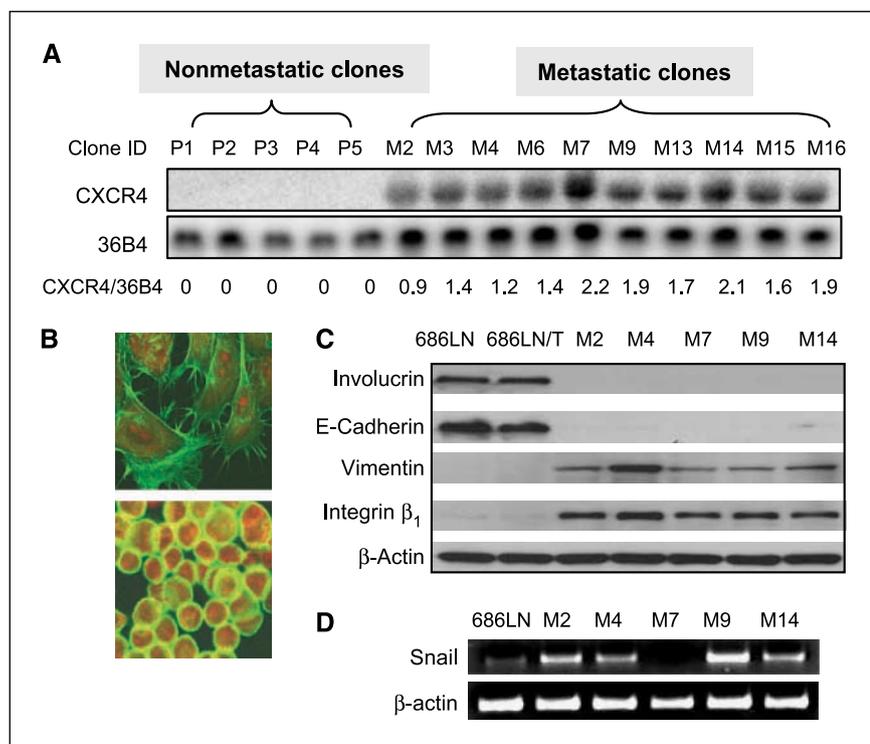

Figure 1. Features of metastatic SCCHN subclones. *A*, CXCR4 levels are elevated in metastatic SCCHN subclones compared with nonmetastatic clones as determined by Northern blot analysis. The average ratio of CXCR4 over human ribosomal phosphoprotein 36B4 (loading control) was 1.64 ± 0.42 (arbitrary unit) for metastatic clones, whereas CXCR4 was not detectable in any of the nonmetastatic clones. *B*, the metastatic SCCHN cells have poorly differentiated phenotypes compared with their parental cells. Phalloidin staining (*green*) reveals striking differences in the actin cytoskeleton and cell adhesions. Nuclear counterstaining (*red*). *C*, Western blot analysis data show the protein expression levels of various EMT biomarkers in metastatic clones. 686LN represents the protein lysate obtained from the original cell line and 686LN/T represents the protein lysate obtained from tumors *in vivo*. Whereas parental cells (686LN and 686LN/T) express high levels of involucrin and E-cadherin, the metastatic clones (M2, M4, M7, M9, and M14) express high levels of vimentin and integrin β_1. *D*, mRNA levels of Snail, one of the EMT-inducing transcriptional factors, was measured by RT-PCR. β-Actin was used as a loading control.

Table 1. Differential expression of chemokines/chemokine receptors and ILs/IL receptors between metastatic versus nonmetastatic SCCHN

NCBI ID	Gene title	Gene symbol	Fold changes	*P*
NM_000575	IL-1, α	IL1A	−419.51	0
NM_000576	IL-1, β	IL1B	−59.60	0
NM_001511	Chemokine (C-X-C motif) ligand 1	CXCL1	−34.52	0
NM_019618	IL-1 family, member 9	IL1F9	−31.97	0
NM_004633	IL-1 receptor, type II	IL1R2	−17.12	$4.4944e-15$
NM_001562	IL-18 (IFN-γ–inducing factor)	IL18	−6.77	$1.4743e-11$
NM_173841	IL-1 receptor antagonist	IL1RN	−5.55	$3.5929e-14$
NM_002185	IL-7 receptor	IL7R	−3.44	$2.0053e-07$
NM_002189	IL-15 receptor, α	IL15RA	−2.15	$2.2421e-10$
NM_002993	Chemokine (C-X-C motif) ligand 6	CXCL6	−2.09	$1.6221e-08$
NM_000877	IL-1 receptor, type I	IL1R1	1.73	$8.2312e-05$
BX537762	IL-1 receptor-associated kinase 1 binding protein 1	IRAK1BP1	2.08	$1.9731e-11$
NM_001560	IL-13 receptor, α1	IL13RA1	2.32	$3.9523e-11$
NM_000418	IL-4 receptor	IL4R	2.35	$4.7612e-09$
NM_004843	IL-27 receptor, α	IL27RA	3.06	$2.5659e-13$
NM_002089	Chemokine (C-X-C motif) ligand 2	CXCL2	4.94	$3.4889e-08$
NM_004843	IL-27 receptor, α	IL27RA	5.78	$9.4763e-11$
NM_003965	Chemokine (C-C motif) receptor-like 2	CCRL2	6.04	$2.8468e-09$
NM_018725	IL-17 receptor B	IL17RB	11.11	0
NM_172174	IL-15	IL15	15.39	0
NM_000600	IL-6 (IFN, β2)	IL6	17.24	$7.59e-11$
NM_001008540	Chemokine (C-X-C motif) receptor 4	CXCR4	244.38	0

Abbreviation: NCBI, National Center for Biotechnology Information.

suppressed by the addition of 100 nmol/L TN14003. The scrambled control peptide did not inhibit Matrigel invasion (Supplementary Data). CXCR4⁻ nonmetastatic cells failed to invade through the Matrigel even in the presence of SDF-1α in the bottom chamber (data not shown).

To assess the effect of CXCR4 inhibition on SCCHN *in vivo*, we used an orthotopic animal model for SCCHN in which luciferase-positive 686LN-Ms cells were implanted submandibularly into nude mice. Beginning on the 8th day after the initial tumor cell injection, two groups of mice were treated with either control peptide (2 mg/kg) or the CXCR4 antagonistic peptide TN14003 (2 mg/kg) by i.p. injection thrice weekly for 27 days (Fig. 2). Tumor growth at the primary site was monitored by BLI at 2 weeks post-treatment. Representative BLI images from each group are shown in Fig. 3*A*. These data reveal that the CXCR4 antagonist suppressed primary tumor growth. Because BLI images are qualitative, not quantitative, we also tracked the changes in tumor volume by caliper measurements on the 14th, 19th, 24th, and 28th day of treatment for the 2 mg/kg TN14003 and the control groups. The tumor volumes of the TN14003-treated and control groups were 286 ± 133 and 518 ± 173 on day 22, 560 ± 223 and 1,247 ± 305 on day 28, 809 ± 256 and 1,705 ± 587 on day 32, and 951 ± 278 and 2,185 ± 746 mm³ on day 35 after the tumor cell injection, respectively (Fig. 3*B*). These data indicate that the CXCR4 antagonist delayed tumor growth at the early stage of tumor development, which suggests the potential involvement of the interaction between CXCR4 and SDF-1 in tumor angiogenesis. To determine whether the suppression of primary tumor growth was a result of an antiangiogenic effect of the CXCR4 antagonist (i.e., inhibition of the formation of tumor microvessels), we did

immunohistochemistry of CD31 on primary tumor tissue sections. Microvessel density (MVD) was calculated by averaging the CD31⁺ microvessels of primary tumors in each group (*n* = 6). As expected, we observed a significant reduction of MVD in the tumors of CXCR4 antagonist-treated mice compared with those of the control group (*P* < 0.0001; Fig. 3*C*).

Blocking CXCR4 inhibits lung metastasis of SCCHN in the orthotopic animal model. The lungs from the mice shown in
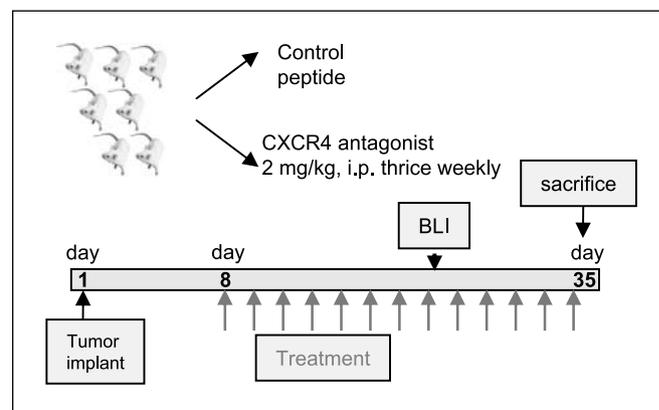

Figure 2. Orthotopic animal experiment scheme. The orthotopic animal experiment was done with six mice per group. Nude mice were injected submandibularly with 5×10^5 SCCHN cells suspended in 50 μL PBS to mylohyoid muscle. The i.p. treatment of TN14003 and the control peptide (2 mg/kg) started 8 d after the tumor injection and lasted for an additional 27 d. BLI was done initially on day 8 before the treatment began to evenly distribute the tumor sizes between the two groups; BLI was also taken 2 wk after the treatment initiation.
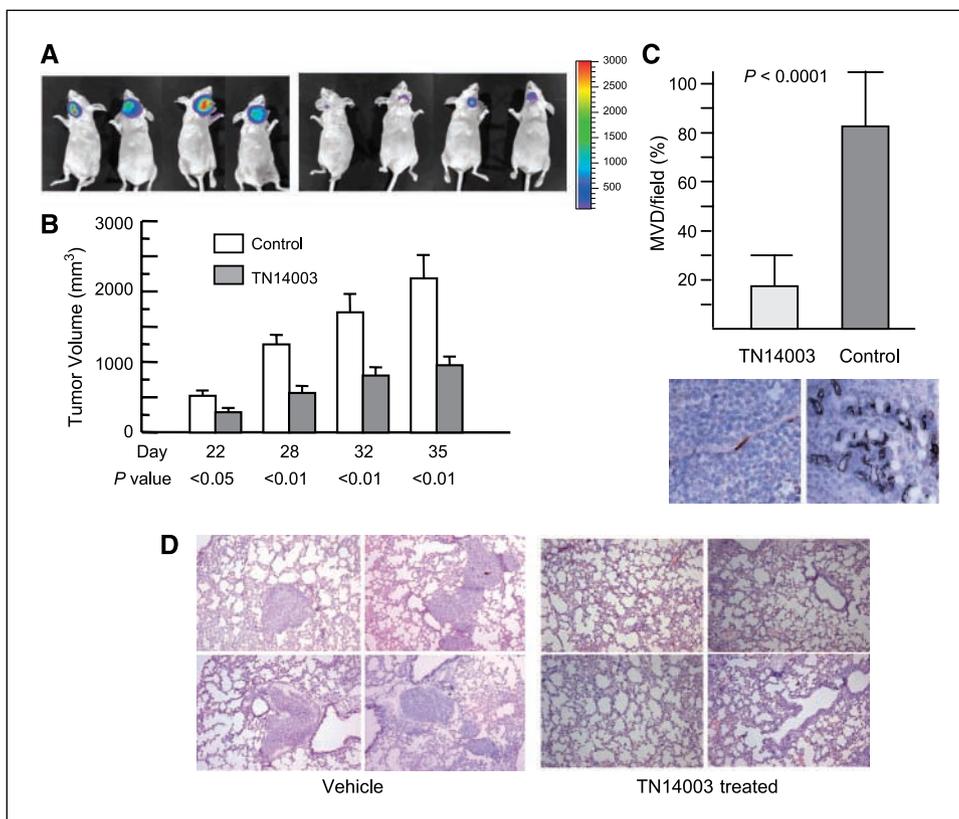
Figure 3. Blockade of tumor growth at the primary site in an orthotopic animal model by CXCR4 antagonist TN14003. *A,* representative BLI images from each group showed that CXCR4 antagonist treatment suppressed primary tumor growth. Bioluminescence intensity (*right*). *B,* tumor volumes were measured by caliper from TN14003-treated versus control group for days 22, 28, 32, and 35 following the tumor cell injection (*n* = 6 per group). Note that the animals were divided into two groups to have even distribution of tumor sizes before treatment initiation based on BLI results and their appearance. This experiment was repeated once more to confirm the antitumor effect of CXCR4 on primary tumors. *C,* immunohistochemistry of CD31 on representative primary tumor tissue sections. The MVD was calculated by averaging numbers of CD31^{+} microvessels of primary tumors in each group (*n* = 6). A significant reduction in MVD was seen in the tumors of CXCR4 antagonist-treated mice compared with those of the control group (*P* < 0.0001). *D,* the lungs from the orthotopic animal model for SCCHN were collected and stained with H&E to find micrometastases. *Left,* mouse lung metastases from the control group; *right,* mouse lungs with normal morphology. The H&E data revealed that none of the treated lungs contained metastatic colonies, whereas control lungs contained metastatic colonies (*dense blue patches*).

Fig. 3*A* were collected, fixed, and paraffin embedded. The whole lungs were sectioned into 6-μm slices; every 10th slice was stained with H&E and analyzed for the presence of metastases. None of the lungs from mice treated with the anti-CXCR4 peptide contained metastatic colonies, whereas lungs from control mice contained numerous metastatic colonies (Fig. 3*D*). These results indicate that blocking CXCR4 completely inhibited lung metastasis in an orthotopic animal model of SCCHN. Decreased metastasis to the lung in CXCR4 antagonist-treated animals could be due to either failure to metastasize or to the cytotoxicity of the treatment. To determine the cytotoxicity of the CXCR4 antagonist, metastatic 686LN cells were treated with different concentrations of the antagonist and its effects on proliferation were determined. The CXCR4 antagonist did not affect cell proliferation even at a high concentrations *in vitro* (data not shown). Thus, it is unlikely that CXCR4 antagonist-treated animals did not form large primary tumors or metastasis due to the cytotoxic effect of the CXCR4 antagonist.

Blocking CXCR4 inhibits lung metastasis in an experimental metastatic animal model. Because primary tumor size is known to correlate with metastasis rate (21), it was conceivable that the reduction in primary tumor size in treated versus control animals accounted for the inhibition of lung metastasis observed. To determine whether the CXCR4 antagonist could reduce the rate of lung metastasis formation independent of size difference of primary tumors, we carried out an independent experiment in which 2×10^6 metastatic 686LN cells were injected through the tail vein, thus resulting in the same number of cells circulating in the bloodstream of control versus treated animals. In 30 days, cells metastasized to the lungs in the control peptide-treated group, whereas they failed to metastasize to any organ in the CXCR4

antagonist-treated group as determined by noninvasive [18F]FDG-PET (Fig. 4). Figure 4 is a maximum intensity projection generated from six mice in each group. The chest area is significantly brighter in each mouse of the control group (Fig. 4, *left*) than any of the mice in the TN14003-treated group (Fig. 4, *right*). The SUV$_{max}$s of
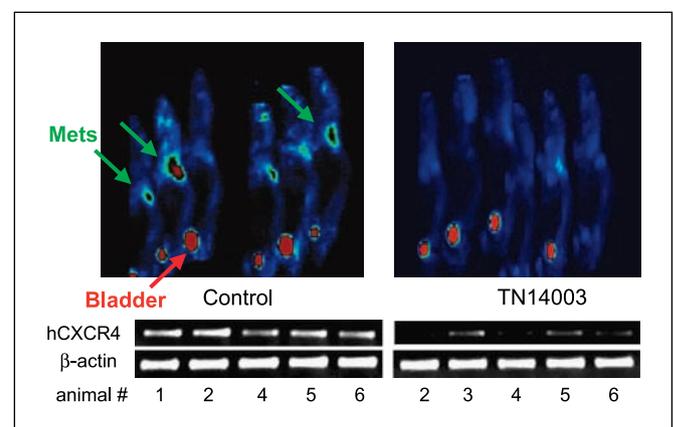

Figure 4. Blocking CXCR4 blocks lung metastasis in SCCHN animal models. An independent experiment was carried out to examine whether blocking CXCR4 will inhibit lung metastases in an experimental metastatic animal model. Noninvasive [18F]FDG-PET images from each group revealed lung metastases (*Mets*) in most mice in the control group (*left*), whereas significantly fewer metastases were found in the CXCR4 antagonist-treated group (*right*). FDG-PET results were verified by RT-PCR using primers recognizing human CXCR4, but not mouse CXCR4. The mouse number is shown below the gel photographs. Immediately following the PET scan, two mice died, one from the control group (#3) and the other from the TN14003-treated group (#1). Thus, RT-PCR results are shown for five mice each from two groups. These experiments were repeated to confirm the results (*n* = 6 for each group for the first set of experiments; *n* = 5 for the second set of experiments).

the lung area were 7.2, 9.8, 2.5, 7.0, 5.9, and 8.2 for the control group and 2.1, 2.0, 1.9, 2.2, 3.1, and 2.5 for the CXCR4 antagonist-treated group (Fig. 4). Collectively, these images show that FDG uptake is much higher in lungs from mice in the control group compared with mice from the CXCR4 antagonist-treated group. Thus, FDG-PET images showed that the control group had a significantly greater number of lung metastases than the TN14003-treated mice. High FDG uptake can also be seen in the bladder in most mice due to the secretion of FDG through the bladder, which varies among individual animals. Next morning, the lungs from the mice shown in Fig. 4 were collected and fresh frozen in OCT compound. We were able to collect lungs from five mice per group due to one death in each group following the FDG-PET scan. The lungs were processed to obtain total RNA, which was used to determine human CXCR4 mRNA levels in the lungs of each mouse by RT-PCR using primers that specifically recognized human CXCR4, but not mouse CXCR4. RT-PCR analyses confirmed that there was high expression of human CXCR4 mRNA in metastasis-infiltrated lungs of the nude mice injected with the control peptide (Fig. 4). In contrast, there was a lower expression of human CXCR4 in the lungs of the CXCR4 antagonist-treated mice, indicating fewer metastases. These results show that blocking CXCR4 prevented metastasis in an experimental animal model of SCCHN, in which equal numbers of metastatic tumor cells were in the circulation of animals in the two comparison groups. Again, this confirms that CXCR4 plays a key role in SCCHN metastasis.

In summary, results from both the orthotopic and the experimental models for metastasis showed that blocking CXCR4 suppressed the growth of primary tumors and prevented lung metastasis of SCCHN cells.

Discussion

The present study investigated the antiangiogenic and antimetastatic activity of a small synthetic peptide against CXCR4, a chemokine receptor that is suggested to contribute to the metastasis of several types of cancers (22–29). Previously, Wang et al. (18) reported that metastatic cells derived from the metastatic mouse model of SCCHN expressed elevated levels of CCR7, another chemokine receptor. We observed that metastatic clones of SCCHN established from the same model expressed high levels of CXCR4, whereas nonmetastatic parental clones established from the primary tumor of the same model did not. This suggests that CXCR4 is required for the metastatic process.

Using our unique SCCHN orthotopic animal model, the CXCR4 antagonist delayed tumor growth at the early stage of tumor development, which suggested the potential involvement of the interaction between CXCR4 and SDF-1 in tumor angiogenesis. In addition, blocking CXCR4/SDF-1 interaction completely inhibited lung metastasis. However, because the incidence of metastases is known to correlate with primary tumor size, it was possible that in this animal model, the antitumor effect of the CXCR4 antagonist rather than an antimetastatic effect accounted for the lack of metastases in control animals. Thus, we carried out an independent experiment in which the same numbers of metastatic 686LN cells were circulating in the bloodstream of control versus treated animals. In this experimental metastasis animal model, ability to home to the lungs is the major factor determining the success rate of lung metastasis formation. The extent of lung metastasis was determined by PET scanning with [^{18}F]FDG. FDG-PET scans of the lungs revealed that CXCR4 antagonist treatment significantly lowered metastasis, most likely due to prevention of homing to the lungs where SDF-1 stromal levels are high. These findings were further supported by the detection of much lower levels of human CXCR4 mRNA in CXCR4 antagonist-treated lungs compared with control peptide-treated lungs, suggesting that inhibiting CXCR4 blocked SCCHN cancer cells from forming lung metastasis.

The mechanism by which CXCR4/SDF-1 promotes tumorigenesis may well depend on its critical role in tumor angiogenesis, which is crucial for tumor initiation and growth (11). Indeed, we observed a significant reduction in CD31$^+$ MVD in the tumors of CXCR4 antagonist-treated mice compared with those of the control group. We determined VEGF mRNA levels in 686LN parental and metastatic cells and found that they expressed the same high VEGF levels *in vitro* (Supplementary Data). However, we were unsuccessful in measuring VEGF mRNA levels from the tumors that were treated with CXCR4 antagonist compared with untreated (the RNA was of insufficient quality for real-time RT-PCR). Although we found similar levels of VEGF mRNA in metastatic versus nonmetastatic cell lines, independent studies observed that reducing CXCR4 levels by small interfering RNA transfection reduced VEGF mRNA levels and VEGF promoter activity in various cell lines (breast cancer cells, glioma cells, and SCCHN cells).[5] Thus, the difference in CD31 expression seen in primary tumors between the treated and untreated groups was due to the critical interaction of CXCR4/SDF-1 that affects not only SDF-1–mediated angiogenesis but also VEGF-induced angiogenesis. Our data showing the suppression of primary tumor growth by the CXCR4 antagonist correlate well with its antiangiogenic effect (i.e., the inhibition of microvessel formation in primary tumor tissue sections). On the other hand, hypoxia is a microenvironmental change that occurs in most solid tumors and is a primary inducer of tumor angiogenesis. Staller et al. (30) showed that a von Hippel-Lindau tumor suppressor protein, pVHL, negatively regulates CXCR4 expression through hypoxia-inducible factor-1 (HIF-1). However, we found that HIF-1α mRNA levels did not correlate with metastatic potential nor with CXCR4 levels (Supplementary Data) in the model system used here. Thus, we suspect that the metastatic cells generated in our model acquired CXCR4 overexpression independently of changes in HIF-1α. Because of the prominent vasculature of SCCHN and the dependence of SCCHN on angiogenesis for malignant progression, it is of great interest to investigate the potential therapeutic effects of anti-CXCR4 compounds for SCCHN.

To gain motility and invasiveness, carcinoma cells must shed many of their epithelial phenotypes and undergo a drastic alteration, the EMT (21). An intriguing observation of our metastatic clones was that these cells possessed completely different morphology after *in vivo* selection, which was preserved even when passaged *in vitro*. Phalloidin staining of the 686LN-Ms cells revealed a loss of organized actin stress fibers, indicating that the metastatic clones had lost the characteristics of epithelial cells. In addition, the 686LN cells expressed high levels of the epithelial markers involucrin and E-cadherin, but low levels of the mesenchymal markers integrin β$_1$ and vimentin, whereas the metastatic clones showed the opposite pattern. The EMT-inducing transcription factors Slug, Snail, and Twist, which regulate the expression of tumor suppressors, such as E-cadherin, were examined in these metastatic clones compared with their counterparts.

---

[5] Unpublished data.

In our SCCHN system, Snail was significantly elevated in all but one of the metastatic clones. Consistent with our observations, Snail was reported to play a key role in Akt-induced EMT in SCCHN cell lines SCC13 and SCC15 (31). Furthermore, Onoue et al. (32) reported recently that SDF-1/CXCR4 induces EMT via activation of the phosphatidylinositol 3-kinase/Akt pathway in oral SCC cells.

This study showed that our metastatic animal model provides a unique model system to study the microenvironment of SCCHN metastasis. Microarray data generated using this model revealed several genes encoding chemokines, ILs, and their receptors that were differentially expressed between nonmetastatic parental cells and metastatic cells. Among them, CXCR4 and IL-6 were significantly elevated in metastatic cells compared with their counterpart. Expression of IL-6, a proinvasive cytokine, has been reported to be greater in cell lines with a significant $CD44^+/CD24^-$ population than in other cell lines (33). $CD44^+/CD24^-$ is a popular biomarker for breast cancer stem cells, and this $CD44^+/CD24^-$ subpopulation has the unique ability to invade, home, and proliferate at sites of metastasis. IL-6 has also been shown to play a critical role in bone metastasis formation (34), and numerous reports show that IL-6 plays a significant role in tumor progression and metastasis (35–39). It is intriguing that blocking CXCR4 alone was sufficient to block the metastatic process of SCCHN metastatic cells overexpressing various chemokine and cytokine receptors.

In summary, these data show that blocking CXCR4 reduces primary tumor growth and inhibits lung metastasis of SCCHN cancer in animal models, suggesting that CXCR4 is an excellent target to inhibit tumor progression.

References

1. Kotwall C, Sako K, Razack MS, Rao U, Bakamjian V, Shedd DP. Metastatic patterns in squamous cell cancer of the head and neck. Am J Surg 1987;154:439–42.
2. Morales J, Homey B, Vicari AP, et al. CTACK, a skin-associated chemokine that preferentially attracts skin-homing memory T cells. Proc Natl Acad Sci U S A 1999; 96:14470–5.
3. Homey B, Wang W, Soto H, et al. Cutting edge: the orphan chemokine receptor G protein-coupled receptor-2 (GPR-2, CCR10) binds the skin-associated chemokine CCL27 (CTACK/ALP/ILC). J Immunol 2000;164: 3465–70.
4. Peled A, Petit I, Kollet O, et al. Dependence of human stem cell engraftment and repopulation of NOD/SCID mice on CXCR4. Science 1999;283:845–8.
5. Forster R, Schubel A, Breitfeld D, et al. CCR7 coordinates the primary immune response by establishing functional microenvironments in secondary lymphoid organs. Cell 1999;99:23–33.
6. Feng Y, Broder CC, Kennedy PE, Berger EA. HIV-1 entry cofactor: functional cDNA cloning of a seven-transmembrane, G protein-coupled receptor. Science 1996;272:872–7.
7. Davis CB, Dikic I, Unutmaz D, et al. Signal transduction due to HIV-1 envelope interactions with chemokine receptors CXCR4 or CCR5. J Exp Med 1997;186:1793–4.
8. Zaitseva M, Blauvelt A, Lee S, et al. Expression and function of CCR5 and CXCR4 on human Langerhans cells and macrophages: implications for HIV primary infection. Nat Med 1997;3:1369–75.
9. Sanchez X, Cousins-Hodges B, Aguilar T, Gosselink P, Lu Z, Navarro J. Activation of HIV-1 coreceptor (CXCR4) mediates myelosuppression. J Biol Chem 1997;272: 27529–31.
10. Chen WJ, Jayawickreme C, Watson C, et al. Recombinant human CXC-chemokine receptor-4 in melanophores are linked to Gi protein: seven transmembrane coreceptors for human immunodeficiency virus entry into cells. Mol Pharmacol 1998;53:177–81.
11. Guleng B, Tateishi K, Ohta M, et al. Blockade of the stromal cell-derived factor-1/CXCR4 axis attenuates *in vivo* tumor growth by inhibiting angiogenesis in a vascular endothelial growth factor-independent manner. Cancer Res 2005;65:5864–71.
12. Majka M, Janowska-Wieczorek A, Ratajczak J, et al. Stromal-derived factor 1 and thrombopoietin regulate distinct aspects of human megakaryopoiesis. Blood 2000;96:4142–51.
13. Majka M, Ratajczak J, Kowalska MA, Ratajczak MZ.

14. Majka M, Ratajczak J, Lee B, et al. The role of HIV-related chemokine receptors and chemokines in human erythropoiesis *in vitro*. Stem Cells 2000;18:128–38.
15. Kijowski J, Baj-Krzyworzeka M, Majka M, et al. The SDF-1-CXCR4 axis stimulates VEGF secretion and activates integrins but does not affect proliferation and survival in lymphohematopoietic cells. Stem Cells 2001;19:453–66.
16. Liang Z, Wu T, Lou H, et al. Inhibition of breast cancer metastasis by selective synthetic polypeptide against CXCR4. Cancer Res 2004;64:4302–8.
17. Zhang X, Su L, Pirani AA, et al. Understanding metastatic SCCHN cells from unique genotypes to phenotypes with the aid of an animal model and DNA microarray analysis. Clin Exp Metastasis 2006;23:209–22.
18. Wang J, Xi L, Hunt JL, et al. Expression pattern of chemokine receptor 6 (CCR6) and CCR7 in squamous cell carcinoma of the head and neck identifies a novel metastatic phenotype. Cancer Res 2004;64:1861–6.
19. Truong MT, Erasmus JJ, Munden RF, et al. Focal FDG uptake in mediastinal brown fat mimicking malignancy: a potential pitfall resolved on PET/CT. AJR Am J Roentgenol 2004;183:1127–32.
20. Hamacher K, Coenen HH, Stocklin G. Efficient stereospecific synthesis of no-carrier-added 2-[^{18}F]-fluoro-2-deoxy-D-glucose using aminopolyether supported nucleophilic substitution. J Nucl Med 1986;27:235–8.
21. Weinberg RA. Biology of cancer. 1st ed. New York: Garland Science; 2006.
22. Muller A, Homey B, Soto H, et al. Involvement of chemokine receptors in breast cancer metastasis. Nature 2001;410:50–6.
23. Taichman RS, Cooper C, Keller ET, Pienta KJ, Taichman NS, McCauley LK. Use of the stromal cell-derived factor-1/CXCR4 pathway in prostate cancer metastasis to bone. Cancer Res 2002;62:1832–7.
24. Oonuma T, Morimatsu M, Nakagawa T, et al. Role of CXCR4 and SDF-1 in mammary tumor metastasis in the cat. J Vet Med Sci 2003;65:1069–73.
25. Tamamura H, Hori A, Kanzaki N, et al. T140 analogs as CXCR4 antagonists identified as anti-metastatic agents in the treatment of breast cancer. FEBS Lett 2003;550:79–83.
26. Libura J, Drukala J, Majka M, et al. CXCR4-SDF-1 signaling is active in rhabdomyosarcoma cells and regulates locomotion, chemotaxis, and adhesion. Blood 2002;100:2597–606.

27. Kato M, Kitayama J, Kazama S, Nagawa H. Expression pattern of CXC chemokine receptor-4 is correlated with lymph node metastasis in human invasive ductal carcinoma. Breast Cancer Res 2003;5:R144–50.
28. Kucia M, Reca R, Miekus K, et al. Trafficking of normal stem cells and metastasis of cancer stem cells involve similar mechanisms: pivotal role of the SDF-1-CXCR4 axis. Stem Cells 2005;23:879–94.
29. Yun CC, Sun H, Wang D, et al. LPA2 receptor mediates mitogenic signals in human colon cancer cells. Am J Physiol 2005;289:C2–11.
30. Staller P, Sulitkova J, Lisztwan J, Moch H, Oakeley EJ, Krek W. Chemokine receptor CXCR4 downregulated by von Hippel-Lindau tumour suppressor pVHL. Nature 2003;425:307–11.
31. Grille SJ, Bellacosa A, Upson J, et al. The protein kinase Akt induces epithelial mesenchymal transition and promotes enhanced motility and invasiveness of squamous cell carcinoma lines. Cancer Res 2003;63:2172–8.
32. Onoue T, Uchida D, Begum NM, Tomizuka Y, Yoshida H, Sato M. Epithelial-mesenchymal transition induced by the stromal cell-derived factor-1/CXCR4 system in oral squamous cell carcinoma cells. Int J Oncol 2006;29:1133–8.
33. Sheridan C, Kishimoto H, Fuchs RK, et al. $CD44^+/CD24^-$ breast cancer cells exhibit enhanced invasive properties: an early step necessary for metastasis. Breast Cancer Res 2006;8:R59.
34. Sohara Y, Shimada H, DeClerck YA. Mechanisms of bone invasion and metastasis in human neuroblastoma. Cancer Lett 2005;228:203–9.
35. Hojo H, Sun R, Ono Y, et al. Differential production of interleukin-6 and its close relation to liver metastasis in clones from murine P815 mastocytoma. Cancer Lett 1996;108:55–9.
36. Inoue K, Okabe S, Sueoka E, Sueoka N, Tabei T, Suganuma M. The role of interleukin-6 in inhibition of lung metastasis in subcutaneous tumor-bearing mice. Oncol Rep 2000;7:69–73.
37. Paule B. Interleukin-6 and bone metastasis of renal cancer: molecular bases and therapeutic implications. Prog Urol 2001;11:368–75.
38. Shariat SF, Andrews B, Kattan MW, Kim J, Wheeler TM, Slawin KM. Plasma levels of interleukin-6 and its soluble receptor are associated with prostate cancer progression and metastasis. Urology 2001;58:1008–15.
39. Ueda T, Shimada E, Urakawa T. Serum levels of cytokines in patients with colorectal cancer: possible involvement of interleukin-6 and interleukin-8 in hematogenous metastasis. J Gastroenterol 1994;29:423–9.

Binding of stromal derived factor-1α (SDF-1α) to CXCR4 chemokine receptor in normal human megakaryoblasts but not in platelets induces phosphorylation of mitogen-activated protein kinase p42/44 (MAPK), ELK-1 transcription factor, and serine/threonine kinase AKT. Eur J Haematol 2000;64:164–72.

CXC Chemokine Receptor-4 Antagonist Blocks Both Growth of Primary Tumor and Metastasis of Head and Neck Cancer in Xenograft Mouse Models

Younghyoun Yoon, Zhongxing Liang, Xin Zhang, et al.

Updated version	Access the most recent version of this article at: http://cancerres.aacrjournals.org/content/67/15/7518
Supplementary Material	Access the most recent supplemental material at: http://cancerres.aacrjournals.org/content/suppl/2007/07/27/67.15.7518.DC1.html

Cited articles	This article cites 38 articles, 15 of which you can access for free at: http://cancerres.aacrjournals.org/content/67/15/7518.full.html#ref-list-1
Citing articles	This article has been cited by 12 HighWire-hosted articles. Access the articles at: http://cancerres.aacrjournals.org/content/67/15/7518.full.html#related-urls

E-mail alerts	Sign up to receive free email-alerts related to this article or journal.
Reprints and Subscriptions	To order reprints of this article or to subscribe to the journal, contact the AACR Publications Department at pubs@aacr.org.
Permissions	To request permission to re-use all or part of this article, contact the AACR Publications Department at permissions@aacr.org.